OPEN GEOMECHANICS

Enriching constitutive models with meso-scale behaviour: a thermodynamics-based formulation and examples

Giang Dinh Nguyen [a], *Arash Mir* [a] & *Ha Hong Bui* [b]

[a] *School of Civil, Environmental and Mining Engineering, The University of Adelaide, Australia*

[b] *Department of Civil Engineering, Monash University, Australia.*

Published
25th August 2022
https://doi.org/10.5802/ogeo.12

Edited by
Edward Andò
EPFL Centre for Imaging
École Polytechnique Fédérale de Lausanne

Reviewed by
Stanislaw Pietruszczak
Department of Civil Engineering
McMaster University

Chloé Arson
School of Civil and Environmental Engineering
Georgia Institute of Technology

Correspondence
Giang Dinh Nguyen
School of Civil, Environmental and Mining Engineering, The University of Adelaide, Australia
g.nguyen@adelaide.edu.au
giang.nguyen@trinity.oxon.org

Open Geomechanics is member of the Centre Mersenne for Open Scientific Publishing

Abstract. A generic approach to encapsulating meso scale details and their associated dissipative mechanisms in constitutive models for geomaterials is presented. The focus is the explicit meso-macro link as the basis for developments of constitutive models. These links are usually missing in constitutive modelling of geomaterials, leading to incorrect description of post-localisation behaviour at the constitutive (material) level. In other words, the classical definition of material behaviour associated with a unit volume element, based on conditions of homogenous deformation, ceases to exist once localised failure occurs. Such localisation issues can and should also be dealt with at the constitutive level. The proposed generic thermodynamics-based formulation to integrate meso scale behaviour of localisation band in constitutive models provides a way to connect meso and macro scales so that post-localisation behaviour can be correctly described at the constitutive level. Examples on onset of localisation and post-localisation behaviour are used to demonstrate key features and benefits of the proposed approach.

Keywords. strain localisation, constitutive modelling, geomaterials, meso scale, macro scale, thermodynamics

1. Introduction

Classical constitutive models are formulated on the assumptions of homogeneous deformation and can be used for an arbitrary volume element in the analysis of Boundary Value Problems (BVPs) as long as this volume element is homogeneous in both stress and deformation. However, it has been well known that failure observed experimentally or in the field usually (if not always) involves localisation of deformation. In such cases, the distribution of strains in a volume element is no longer sufficiently uniform to be considered homogeneous, destroying the assumption of homogeneity that formulations of classical constitutive models are based on. In this sense, the problem (specimen failure in experiments) becomes a BVP once localisation of deformation takes place, due to the appearance of a localisation band and its behaviour at a scale (meso scale) lower than the size of the specimen (Labuz and Biolzi 1991). Therefore, post-localisation behaviour cannot be correctly described by a classical constitutive model, due to lack of details, including behaviour and geometrical properties, at the meso scale of the localisation band in such a model. It is noted that the topic of strain localisation and bifurcation in continuum modelling that has been extensively investigated in the literature [Mühlhaus and Vardoulakis, 1987, Neilsen and Schreyer, 1993, Rice and Rudnicki, 1980, Rudnicki and Rice, 1975, Vardoulakis, 1989, Vardoulakis et al., 1978, Vardoulakis and Sulem, 1995] , and it is not the intention of this paper to cover a comprehensive literature review on this topic. Instead the focus is on post-localisation behaviour, where classical continuum models cease to be valid, and how to enhance constitutive models to better deal with post-localisation behaviour.

In the context of analysis of BVPs, any attempt to use classical continuum models in problems involving localised failure requires additional enhancements, called regularisation, to overcome localisation-related issues to assure the meaningful convergence of the numerical solutions with respect to discretisation refinement. Examples of regularisations include the simple scaling of behaviour based on fracture energy used in smeared crack/deformation approach (Cedolin and Bažant 1980, Crook et al. 2006, Zabala and Alonso 2011, Soga et al. 2016), higher order theories that take into account interactions among volume elements described by a constitutive model through an additional integral (nonlocal theories) [Bažant, 1991, Jirásek, 1998, Pijaudier-Cabot and Bažant, 1987] or differential equation (gradient theories) [Chen and Schreyer, 1987, De Borst and Mühlhaus, 1992], or rate-dependent regularisation [Das et al., 2014, Mir et al., 2018]. Other element-based approaches, e.g. Enhanced Assumed Strain (EAS) or Strong Discontinuity Approach (SDA) [Borja, 2000, Jirásek, 2000, Larsson et al., 1996, Oliver, 1996, Oliver et al., 2006], eXtended Finite Element Method – XFEM [Samaniego and Belytschko, 2005, Sanborn and Prévost, 2011, Wells and Sluys, 2001], can also be used to handle localised failure in the analysis of BVPs but need the involvement of a numerical method. Therefore, they are considered out of scope, given our focus on constitutive modelling, and hence not discussed in this paper.

In this study, we aim to develop an approach to deal with localised failure at the constitutive level without requiring the involvement of a numerical method for the solutions of BVPs. This approach is not as sophisticated although not as accurate and comprehensive as higher order methods that always require the involvement of the analysis of BVPs in analysis of localised failure. However, it can provide a direct, one-to-one mapping between the observed features of localised failure and the constitutive models and their parameters, all of which are not always straightforward with other types of regularisations. In addition, its implementation in a mesh-based or mesh-free numerical method for the solutions of BVPs will be straightforward, given it is independent of any characteristics of a numerical method. The role of meso scale failure mechanism in correctly describing post-localisation behaviour is particularly focused on, given this is the missing bit in constitutive modelling of geomaterials that usually prevent a smooth transition from constitutive modelling to analysis of BVPs.

The importance and benefits of integrating meso scale behaviour in constitutive models for geomaterials have been recognised in the literature, although in our opinion not widely popular in the community of constitutive modellers. The majority of constitutive models having been developed and used in geomechanics and geotechnical engineering are not able to describe correctly post-localisation behaviour, making the calibration and validation with experiments involving localised failure not physically meaningful. In this sense, it is essential to make sure the descriptions of constitutive behaviour are physically meaningful and correct first, before any attempts to improve the performance of the models to reproduce experimental results. This has been our focus over the last 10 years on bridging behaviour across a few scales in constitutive modelling and applications in geomechanics [Bui and Nguyen, 2021, Le et al., 2022, 2018, 2019, 2017, Nguyen et al., 2017, Nguyen and Bui, 2020, Nguyen et al., 2012, 2014, 2016a,b, Tran et al., 2019, Wang et al., 2019, 2020]. It has been shown in these papers that adding meso scale behaviour of a localisation band in constitutive modelling of geomatetrials is not only an essential way to describe correctly post-localisation behaviour but also a good approach to incorporate behaviour at a scale lower than meso scale [Le et al., 2019]. Much earlier pioneering work on this issue in constitutive modelling by Pietruszczak and co-authors [Pietruszczak, 1999, Pietruszczak and Haghighat, 2015, Pietruszczak and Mróz, 1981, Pietruszczak and Mroz, 2001, Pietruszczak and Xu, 1995, Xu and Pietruszczak, 1997] are also well recognised and appreciated, although not formulated based on either meso-macro work balance or thermodynamics that can be applicable to a range of constitutive models.

This paper is built on our earlier work mentioned above. A new generic thermodynamic formulation is described for both developments of new and enhancement of existing constitutive models. The demonstrations provided in this paper include (i) stress return algorithm to bridge meso and macro scales, (ii) detection of onset and orientation

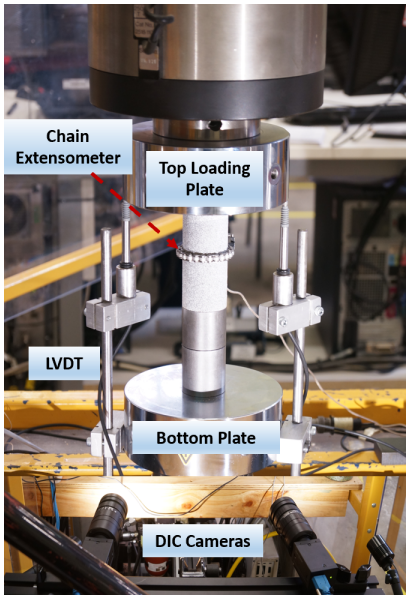

Figure 1. Set-up for uniaxial compression of Hawksbury sandstone specimen.

of localisation band for transition from diffuse to localised failure, (iii) enhancement of an existing model for rocks under different confining pressures using both the proposed two-scale approaches and a rate-dependent regularisation, and (iv) assessment of a two-scale model against both experimental data and numerical results obtained from Finite Element Analysis (FEA) using rate-dependent regularisartion. It is noted that a comprehensive assessment and validation of the proposed approach and models presented is not the intention of this study. Instead, we would like to use the models and obtained results as a means to convey the key message in constitutive modelling of geomaterials: meso-scale behaviour due to localisation should be incorporated in the structure of constitutive models before any attempts to calibrate a model to reproduce experimental results.

Results on failure of sandstone specimens under uniaxial compression are presented in this section to provide a background on localised failure for the theoretical development in the next section. It is noted that this presentation is not a comprehensive one and serves the sole purpose of explaining why meso scale behaviour of localisation band is needed in constitutive modelling of engineering materials.

Cylindrical specimens of 42 mm diameter of Hawkesbury sandstone, with an aspect ratio (height/diameter) of 3.5, are subject to uniaxial compression. Indirect displacement control based on lateral deformation is used to capture snap-back behaviour due to size effect induced by localisation. The rate of lateral deformation obtained from the chain extensometer attached to the specimen (Figure 1) was maintained constant and used as feedback to the loading frame. Three-dimensional Digital Image Correlation (DIC) technique was used to obtain full field strains and their evolutions during deformation of the specimens. Details on the experiment and analysis can be found in our recent papers [Pour et al., 2022, Verma et al., 2021].

The evolution of Von Mises strain on the surface of the specimen is synchronised with its mechanical behaviour and plotted in Figure 2. Despite the snap-back observed in the mechanical response, the evolution of strain localisation is not abrupt, showing a gradual transition from diffuse to localised failure (Fig. 2ii) with a finite thickness localisation band [Pour et al., 2022]. It is noted that due to the chain extensometer in the middle of the specimen (Fig. 1) used to control and capture snap-back response, DIC data are not available in the middle of the specimen, and linear interpolation is used in plotting the strain profiles in Fig. 2ii. The material inhomogeneity can be seen in the fluctuation of strain profiles before peak (Fig. 2ii), while in the post-peak regime (from point "c" in Fig. 2i) the maximum strain in the localisation band gradually reaches a very high level at least one order of magnitude above the magnitude of strain in the outside region. This difference is well beyond the amplitude of strain fluctuation due to material inhomogeneity observed on pre-peak regime. Therefore, assumptions on homogeneity used in continuum mechanics for interpreting experimental data are not valid anymore.

The observed process of strain localisation gradually separates the specimen into two distinct regions each of which follows its own loading path. Unloading with magnitude of strain decreasing can be seen in the region outside the localisation band, while the inelastic loading inside the localisation band gradually results in the separation of the specimen. However, from statics equilibrium, the stresses in these two regions (localisation band and the bulk material outside the band) must be in equilibrium realised in the continuity of stress components normal and tangential to the localisation band. The above observations on strain localisation and internal equilibrium provide a basis for the development of constitutive models that can correctly take into account localisation of deformation underpinning the observed mechanical response of a specimen. This is the focus of this paper.

1.1. Localised failure and kinematic enrichment

As can be seen in Fig. 2, despite very brittle behaviour observed, the thickness of the localisation band can be considered significant compared to the size of the specimen, making the assumption of a finite thickness band reasonable. Due to different responses inside and outside the localisation band, the macro strain ε_{ij} representing the averaged deformation of a volume element consisting of a localisation band can be considered as a volume averaged quantity:

$$\varepsilon_{ij} = (1-f)\varepsilon^o_{ij} + f\varepsilon^i_{ij} \tag{1}$$

The localisation zone can be assumed to take the form of a planar band as usually observed at both lab [Alshibli and Hasan, 2008, Andò et al., 2013, Baud et al., 2004, Charalampidou et al., 2014, Thakur et al., 2017] and field scales [Chemenda, 2011, Mollema and Antonellini, 1996, Sternlof et al., 2005]. Therefore the volume fraction f of this localisation band can be expressed as the ratio between the thickness h of this band and the effective size $H = \frac{V}{S}$ of the volume element containing it (Fig. 3), where S is the surface

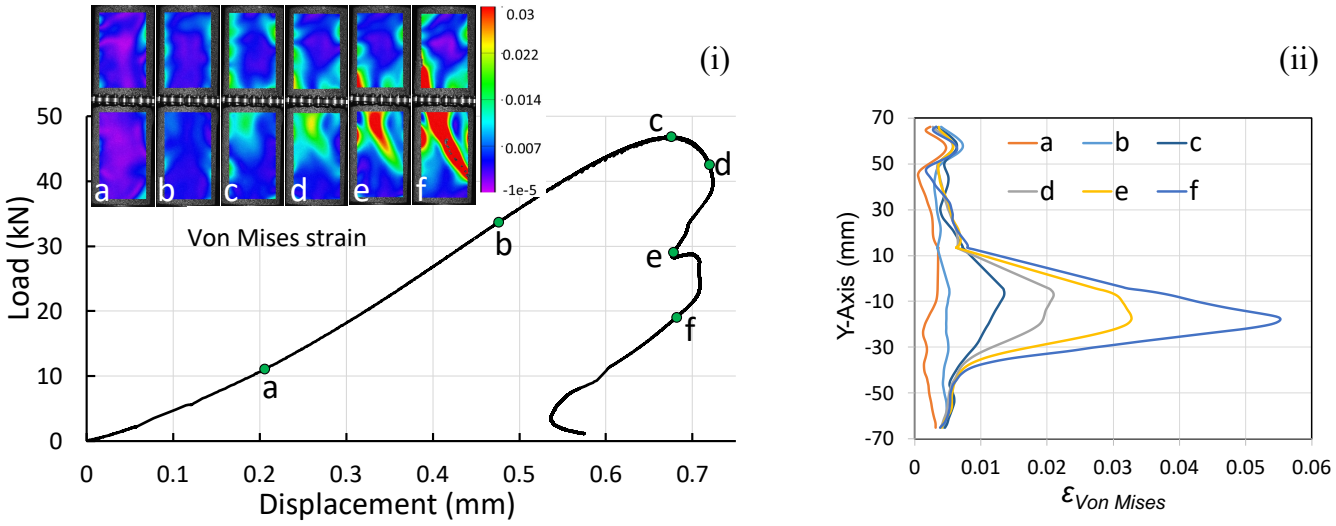

Figure 2. Mechanical responses and evolution of Von Mises strain – (i): load-displacement response with snap-back and evolution of Von Mises strain contour on specimen surface; (ii): evolution of Von Mises strain profile along a vertical line in the middle of the specimen.

area of the localisation zone:

$$f = \frac{Sh}{V} = \frac{Sh}{SH} = \frac{h}{H} \tag{2}$$

Due to localisation and high gradient of strain rate across the boundary of the localisation zone (Fig. 2) the strain rate $\dot{\varepsilon}^i_{ij}$ inside the localisation band can be assumed of following form Borja [2000], Neilsen and Schreyer [1993], Oliver [1996]:

$$\dot{\varepsilon}^i_{ij} = \dot{\varepsilon}^o_{ij} + \frac{1}{h}\left(\dot{u}_i n_j\right)^s \tag{3}$$

where $\dot{\varepsilon}^o_{ij}$ is the homogeneous strain rate outside the localisation band. The superscript "s" in equation (3) indicates symmetrisation. The relative velocity $\dot{u}_i$ between two faces of the localisation band, and normal vector n_j describing the orientation of the localisation band are taken into account in the above equation. From equations (1) and (2), we can express $\dot{\varepsilon}^o_{ij}$, and $\dot{\varepsilon}^i_{ij}$ as:

$$\dot{\varepsilon}^o_{ij} = \dot{\varepsilon}_{ij} - \frac{f}{h}\left(\dot{u}_i n_j\right)^s \tag{4}$$

$$\dot{\varepsilon}^i_{ij} = \dot{\varepsilon}_{ij} + \frac{1-f}{h}\left(\dot{u}_i n_j\right)^s \tag{5}$$

The above equations (4-5) have been used in [Mir, 2017, Nguyen and Bui, 2020, Nguyen et al., 2016b] for developing

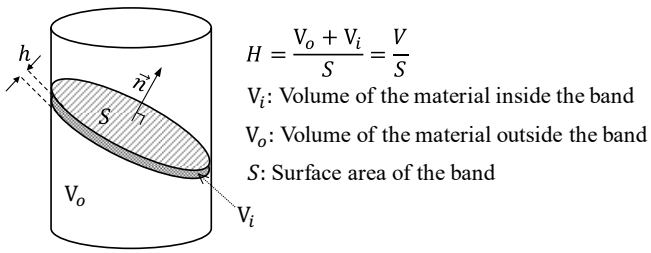

Figure 3. A volume element (with volume V) crossed by a finite thickness localisation band.

constitutive models possessing behaviour at meso scale of the localisation band.

The relationship between macro stress σ_{ij} and macro strain ε_{ij} in this case is not governed by a constitutive law like in classical continuum models, but controlled by the responses inside and outside the localisation band, each of which follows its own constitutive relationship, besides their corresponding sizes. They represent the behaviour below the macro scale of the volume element considered. In this case it is physically reasonable to assume homogeneous behaviour inside the localisation band, governed by two constitutive relationships represented by $\left(\sigma^i_{ij}, \varepsilon^i_{ij}\right)$ and $\left(\sigma^o_{ij}, \varepsilon^o_{ij}\right)$, respectively. It is noted that this assumption is associated with fixed thickness of a localisation band and is a simplification of physical phenomena in which the band thickness has been observed to evolve with its behaviour [Andò, 2013, Andò et al., 2013, Pour et al., 2022, Rattez et al., 2022].

1.2. A Thermodynamics-based formulation

This Section describes enhancements to the thermodynamic framework by [Houlsby and Puzrin, 2000, 2006] originally developed for classical constitutive models based on the assumption of homogeneous deformation. These enhancements are to take into account localisation and behaviour at meso scale so that post-localisation responses can be described correctly by a model enhanced using this proposed two-scale approach. It is noted that a different and more generic thermodynamic approach for constitutive models possessing an embedded localisation band with evolving thickness has been developed in our recent work [Nguyen and Bui, 2020] and can also be used here. However, the use of constraints on kinematic enrichments adopted in this study is a simpler way, suggested by Professor Guy Houlsby of Oxford University during his visit to Adelaide in May 2015, to incorporate useful features to a constitutive model using procedures established beforehand. This use

of constraint to develop thermodynamically consistent two-scale approach has been developed in [Mir, 2017] to derive thermodynamics-based models that can correctly describe both pre- and post-localisation behaviour. A slightly different way is illustrated in this Section, in which the kinematic enrichments in equations (1) and (3) are used as constraints in the energy and dissipation potentials in the current approach. They are rewritten as:

$$C^1_{ij} = \varepsilon_{ij} - (1-f)\varepsilon^o_{ij} - f\varepsilon^i_{ij} = 0 \tag{6}$$

and

$$C^2_{ij} = \dot{\varepsilon}^i_{ij} - \left[\dot{\varepsilon}^o_{ij} + \frac{1}{h}\left(\dot{u}_i n_j\right)^s\right] = 0 \tag{7}$$

where C^1_{ij} and C^2_{ij} are two constraints to be used in the energy and dissipation potentials, respectively. The Helmholtz free energy potential Ψ of a volume element containing a localisation band takes the following volume averaged form:

$$\Psi = (1-f)\Psi^o\left(\varepsilon^o_{ij}, \alpha^o_{ij}\right) + f\Psi^i\left(\varepsilon^i_{ij}, \alpha^i_{ij}\right) + \Lambda^1_{ij}C^1_{ij} \tag{8}$$

where Λ^1_{ij} is the Lagrangian multiplier associated with constraint C^1_{ij}; $\Psi^o\left(\varepsilon^o_{ij}, \alpha^o_{ij}\right)$ and $\Psi^i\left(\varepsilon^i_{ij}, \alpha^i_{ij}\right)$ are the Helmholtz free energies for unit volumes of the regions outside and inside the localisation band, respectively.

The augmented dissipation potential $\widetilde{\Phi}$ of the volume element containing the localisation band is:

$$\widetilde{\Phi} = (1-f)\widetilde{\Phi}^o + f\widetilde{\Phi}^i + \Lambda^2_{ij}C^2_{ij} \tag{9}$$

where Λ^2_{ij} is the Lagrangian multiplier associated with constraint C^2_{ij}. In the above expression, $\widetilde{\Phi}^o$ and $\widetilde{\Phi}^i$ are dissipation potentials written for unit volumes outside and inside the localisation bands, respectively. For rate-independent behaviour considered in this study, they are homogeneous first order functions of the corresponding rate of internal variables, $\dot{\alpha}^i_{ij}$ and $\dot{\alpha}^o_{ij}$. For generality, α^o_{ij} and α^i_{ij} are used as internal variables representing the effects of microstructural evolution at scales lower than the meso scale of the localisation band. It is noted here that α^o_{ij} and α^i_{ij} imply a wide range of internal variables representing the effects of micro-structural changes on macro responses. Examples include plastic strain in plasticity theory, damage variables in damage mechanics [Lubarda and Krajcinovic, 1993, Pijaudier-Cabot and Bažant, 1987], or Breakage variable in Breakage Mechanics [Einav, 2007a,b]. It is noted that Ψ and $\widetilde{\Phi}$ are the energy and dissipation potentials of a unit volume element containing a localisation band, and hence the strains ε^i_{ij}, ε^o_{ij} and displacement jump u_i are considered as internal variables with respect to the macro behaviour of this unit volume element. The sub-scale energy (Ψ^o and Ψ^i) and dissipation potentials ($\widetilde{\Phi}^o$ and $\widetilde{\Phi}^i$) can follow descriptions presented in [Houlsby and Puzrin, 2000, 2006], with specific examples in several publications on continuum models formulated based on this framework.

Following standard procedures in [Houlsby and Puzrin, 2000, 2006], the macro stress σ_{ij} and generalised stresses are obtained from the energy potential (8) as:

$$\sigma_{ij} = \frac{\partial\Psi}{\partial\varepsilon_{ij}} = \Lambda^1_{ij} \tag{10}$$

$$\overline{\chi}^o_{ij} = -\frac{\partial\Psi}{\partial\alpha^o_{ij}} = -(1-f)\frac{\partial\Psi^o}{\partial\alpha^o_{ij}} \tag{11}$$

$$\overline{\chi}^i_{ij} = -\frac{\partial\Psi}{\partial\alpha^i_{ij}} = -f\frac{\partial\Psi^i}{\partial\alpha^i_{ij}} \tag{12}$$

$$\overline{\chi}^{\varepsilon^i}_{ij} = -\frac{\partial\Psi}{\partial\varepsilon^i_{ij}} = -f\frac{\partial\Psi^i}{\partial\varepsilon^i_{ij}} + f\Lambda^1_{ij} \tag{13}$$

$$\overline{\chi}^{\varepsilon^o}_{ij} = -\frac{\partial\Psi}{\partial\varepsilon^o_{ij}} = -(1-f)\frac{\partial\Psi^o}{\partial\varepsilon^o_{ij}} + (1-f)\Lambda^1_{ij} \tag{14}$$

$$\overline{\chi}^u_i = -\frac{\partial\Psi}{\partial u_i} = 0 \tag{15}$$

In the above expressions, $\overline{\chi}^o_{ij}$, $\overline{\chi}^i_{ij}$, $\overline{\chi}^{\varepsilon^i}_{ij}$, $\overline{\chi}^{\varepsilon^o}_{ij}$, and $\overline{\chi}^u_i$ are the generalised stresses associated with α^o_{ij}, α^i_{ij}, ε^i_{ij}, ε^o_{ij}, and u_i, respectively. From the augmented dissipation potential (9), we obtain the following dissipative generalised stresses χ^o_{ij}, χ^i_{ij}, $\chi^{\varepsilon^i}_{ij}$, $\chi^{\varepsilon^o}_{ij}$, and χ^u_i:

$$\chi^o_{ij} = \frac{\partial\widetilde{\Phi}}{\partial\dot{\alpha}^o_{ij}} = (1-f)\frac{\partial\widetilde{\Phi}^o}{\partial\dot{\alpha}^o_{ij}} \tag{16}$$

$$\chi^i_{ij} = \frac{\partial\widetilde{\Phi}}{\partial\dot{\alpha}^i_{ij}} = f\frac{\partial\widetilde{\Phi}^i}{\partial\dot{\alpha}^i_{ij}} \tag{17}$$

$$\chi^{\varepsilon^i}_{ij} = \frac{\partial\widetilde{\Phi}}{\partial\dot{\varepsilon}^i_{ij}} = \Lambda^2_{ij} \tag{18}$$

$$\chi^{\varepsilon^o}_{ij} = \frac{\partial\widetilde{\Phi}}{\partial\dot{\varepsilon}^o_{ij}} = -\Lambda^2_{ij} \tag{19}$$

$$\chi^u_i = \frac{\partial\widetilde{\Phi}}{\partial\dot{u}_i} = \frac{f}{h}\Lambda^2_{ij}n_j \tag{20}$$

We consider at first two Ziegler's orthogonality conditions [Houlsby and Puzrin, 2000, Ziegler, 1983] $\overline{\chi}^o_{ij} = \chi^o_{ij}$ and $\overline{\chi}^i_{ij} = \chi^i_{ij}$. Using equations (11, 12) and (16, 17) these two orthogonality conditions lead to the following expressions:

$$-\frac{\partial\Psi^o}{\partial\alpha^o_{ij}} = \frac{\partial\widetilde{\Phi}^o}{\partial\dot{\alpha}^o_{ij}} \tag{21}$$

$$-\frac{\partial\Psi^i}{\partial\alpha^i_{ij}} = \frac{\partial\widetilde{\Phi}^i}{\partial\dot{\alpha}^i_{ij}} \tag{22}$$

The above are in fact Ziegler's orthogonality conditions for the formulations of two sub-scale models for formulating constitutive responses outside (described by Ψ^o and $\widetilde{\Phi}^o$) and inside the localisation band (described by Ψ^i and $\widetilde{\Phi}^i$).

It can be seen from equations (18) and (19) that $\chi^{\varepsilon^i}_{ij} = -\chi^{\varepsilon^o}_{ij} = \Lambda^2_{ij}$. Using this together with (10) for Ziegler's orthogonality conditions $\overline{\chi}^{\varepsilon^i}_{ij} = \chi^{\varepsilon^i}_{ij}$ and $\overline{\chi}^{\varepsilon^o}_{ij} = \chi^{\varepsilon^o}_{ij}$, we obtain:

$$-f\frac{\partial\Psi^i}{\partial\varepsilon^i_{ij}} + f\sigma_{ij} = (1-f)\frac{\partial\Psi^o}{\partial\varepsilon^o_{ij}} - (1-f)\sigma_{ij} \tag{23}$$

Given Ψ^i and Ψ^o as Helmholtz free energy potentials for regions inside and outside the localisation band, the corresponding stresses σ^i_{ij} and σ^o_{ij} can be expressed as:

$$\sigma^i_{ij} = \frac{\partial\Psi^i}{\partial\varepsilon^i_{ij}} \tag{24}$$

$$\sigma^o_{ij} = \frac{\partial \Psi^o}{\partial \varepsilon^o_{ij}} \tag{25}$$

Equation (23) becomes:

$$\sigma_{ij} = (1-f)\sigma^o_{ij} + f\sigma^i_{ij} \tag{26}$$

which is the volume averaged stress that has also been obtained using the balance of mechanical work produced by macro and meso quantities [Nguyen et al., 2016b].

From equations (15) and (20), Ziegler's orthogonality condition in the form of $\overline{\chi}^u_i = \chi^u_i$ leads to

$$\Lambda^2_{ij} n_j = 0 \tag{27}$$

Using the above condition for Ziegler's orthogonality conditions $\overline{\chi}^{\varepsilon^i}_{ij} = \chi^{\varepsilon^i}_{ij}$ and $\overline{\chi}^{\varepsilon^o}_{ij} = \chi^{\varepsilon^o}_{ij}$, we obtain:

$$\overline{\chi}^{\varepsilon^i}_{ij} n_j = -f\frac{\partial \Psi^i}{\partial \varepsilon^i_{ij}} n_j + f\sigma_{ij} n_j = \chi^{\varepsilon^i}_{ij} n_j = \Lambda^2_{ij} n_j = 0 \tag{28}$$

$$\begin{aligned}\overline{\chi}^{\varepsilon^o}_{ij} n_j &= -(1-f)\frac{\partial \Psi^o}{\partial \varepsilon^o_{ij}} n_j + (1-f)\sigma_{ij} n_j \\ &= \chi^{\varepsilon^o}_{ij} n_j = \Lambda^2_{ij} n_j = 0\end{aligned} \tag{29}$$

The above two equations lead to the following traction continuity condition that has also been obtained in [Nguyen et al., 2016b] using a different approach based on the balance of work.

$$\sigma^o_{ij} n_j = \sigma^i_{ij} n_j = \sigma_{ij} n_j \tag{30}$$

Table 1 summarises the results obtained from the generic formulation.

As can be seen, conditions to obtain constitutive models for homogeneous behaviour inside and outside the localisation band, based on explicitly defined energy (Ψ^i, and Ψ^o) and dissipation potentials ($\widetilde{\Phi}^i$, and $\widetilde{\Phi}^o$), are recovered in this generic formulation. In particular, for given energy potentials Ψ^x and $\widetilde{\Phi}^x$ ("x" stands for "i" or "o") and internal variable α^x_{ij}, the orthogonality conditions $-\frac{\partial \Psi^x}{\partial \alpha^x_{ij}} = \frac{\partial \widetilde{\Phi}^x}{\partial \dot{\alpha}^x_{ij}}$ needed for the formulation of a constitutive model based on the framework by Houlsby and Puzrin [Houlsby and Puzrin, 2000] can be recovered from the above approach. Therefore, formulations of constitutive models for responses inside and outside the localisation band can follow standard procedures established in Houlsby and Puzrin [Houlsby and Puzrin, 2000]. In other words, these models for sub-scale behaviour can be formulated independently, and then combined using the volume-averaged macro stress and traction continuity condition to form the behaviour of a volume element crossed by a localisation band. In this case, the macro response of the volume element containing the band is governed by the behaviour of the localisation band, including its thickness and orientation, together with the behaviour and size of the zone outside this band. The computational algorithms for both macro tangent stiffness and stress return will be described in next sub-sections to give the readers a clearer idea about how to connect the responses inside and outside the localisation zone. The readers can also refer to our previous papers [Le et al., 2018, 2019, 2017, Tran et al., 2019, Wang et al., 2019, 2020] for details and examples on other two-scale models with a localisation band idealised as a zero-thickness surface that can be described by a cohesive-frictional model.

1.3. Computational aspects

Algorithms to connect responses at different scales are essential for the assessment of the model performance and numerical analysis. They are presented here for the sake of completeness given they are not the key focus and have been presented in our earlier works [Bui and Nguyen, 2021, Mir, 2017, Nguyen et al., 2017, Nguyen and Bui, 2020, Nguyen et al., 2016b]. The responses inside and outside the band together with their associated sizes in this case constitute the behaviour of the model. The macro behaviour can only be obtained using its lower scale responses and their interactions through the internal equilibrium condition. This is different from classical models given meso-macro connections are needed for the stress return algorithm and formulation of tangent stiffness, besides the regular stress return routines for responses inside and outside the localisation band. Such connections are paid attention to in this study, leaving regular stress return algorithms for a classical continuum model outside the scope of this paper. For this reason, the incremental behaviour of a unit volume element outside and inside the localisation zone can assume the following generic forms:

$$\dot{\sigma}^o_{ij} = D^o_{ijkl}\dot{\varepsilon}^o_{ij} \tag{31}$$

$$\dot{\sigma}^i_{ij} = D^i_{ijkl}\dot{\varepsilon}^i_{ij} \tag{32}$$

where $D^o_{ijkl}\left(\sigma^o_{ij}, \alpha^o_{ij}\right)$ and $D^i_{ijkl}\left(\sigma^i_{ij}, \alpha^i_{ij}\right)$ are the tangent stiffness tensors depending on the corresponding stress state and internal variables. It is noted that for rate-independent behaviour in this paper, the pseudo rate form is used for convenience. The above constitutive equations are generic incremental relationships and any stress return algorithms can be used to obtain incremental stress tensor from a given incremental strain tensor. The meso-macro stress return algorithms and formulation of tangent stiffness are based on the following relationships linking macro with meso quantities:

$$\sigma_{ij} = (1-f)\sigma^o_{ij} + f\sigma^i_{ij} \tag{33}$$

$$\sigma^o_{ij} n_j = \sigma^i_{ij} n_j = \sigma_{ij} n_j \tag{34}$$

$$\dot{\varepsilon}^o_{ij} = \dot{\varepsilon}_{ij} - \frac{f}{h}\left(\dot{u}_i n_j\right)^s \tag{35}$$

$$\dot{\varepsilon}^i_{ij} = \dot{\varepsilon}_{ij} + \frac{1-f}{h}\left(\dot{u}_i n_j\right)^s \tag{36}$$

These equations are rewritten and summarised here for clarity and ease of following, given they can be used directly for computational algorithms for any existing constitutive models. The whole process of deriving the tangent stiffness and developing stress return algorithm is based on generic constitutive relationships and hence the results in the following sub-sections are applicable to any existing models and loading conditions.

Table 1. Summary of results from the generic formulation.

Macro	Inside the band	Outside the band
Macro stress: $\sigma_{ij} = (1-f)\sigma^o_{ij} + f\sigma^i_{ij}$ Internal equilibrium: $\sigma^o_{ij} n_j = \sigma^i_{ij} n_j = \sigma_{ij} n_j$	Energy potentials Ψ^i and $\widetilde{\Phi}^i$ Internal variable α^i_{ij} $\sigma^i_{ij} = \frac{\partial \Psi^i}{\partial \varepsilon^i_{ij}}$ $-\frac{\partial \Psi^i}{\partial \alpha^i_{ij}} = \frac{\partial \widetilde{\Phi}^i}{\partial \dot{\alpha}^i_{ij}}$	Energy potentials Ψ^o and $\widetilde{\Phi}^o$ Internal variable α^o_{ij} $\sigma^o_{ij} = \frac{\partial \Psi^o}{\partial \varepsilon^o_{ij}}$ $-\frac{\partial \Psi^o}{\partial \alpha^o_{ij}} = \frac{\partial \widetilde{\Phi}^o}{\partial \dot{\alpha}^o_{ij}}$

1.3.1. Tangent stiffness

Substituting the incremental stress-strain relationships (31-32) in the internal equilibrium (34) written in incremental form, we obtain:

$$\left(D^o_{ijkl}\dot{\varepsilon}^o_{kl} - D^i_{ijkl}\dot{\varepsilon}^i_{kl}\right) n_j = 0 \tag{37}$$

The above equation implies that the orientation of the band does not evolve with deformation. Using the meso-macro links between strains (35-36), we can expand (37) to obtain:

$$D^o_{ijkl}\left[\dot{\varepsilon}_{kl} - \frac{f}{h}(\dot{u}_k n_l)^s\right] n_j - D^i_{ijkl}\left[\dot{\varepsilon}_{kl} + \frac{1-f}{h}(\dot{u}_k n_l)^s\right] n_j = 0 \tag{38}$$

The above can be rearranged to:

$$\left(D^o_{ijkl} - D^i_{ijkl}\right)\dot{\varepsilon}_{kl} n_j - \left[\frac{f}{h}D^o_{ijkl} n_l n_j + \frac{1-f}{h}D^i_{ijkl} n_l n_j\right]\dot{u}_k = 0 \tag{39}$$

Therefore, given the macro strain rate $\dot{\varepsilon}_{ij}$, the velocity jump $\dot{u}_k$ can be obtained in the form:

$$\dot{u}_k = C_{ik}{}^{-1}\left(D^o_{ijmn} - D^i_{ijmn}\right)\dot{\varepsilon}_{mn} n_j \tag{40}$$

where

$$C_{ik} = \frac{f}{h}D^o_{ijkl} n_l n_j + \frac{1-f}{h}D^i_{ijkl} n_l n_j \tag{41}$$

plays the role of the localisation or acoustic tensor [Rice and Rudnicki, 1980, Rudnicki and Rice, 1975] that contains both meso scale behaviour and geometrical properties.

Using (35-36) and (40), we can obtain the strain rates outside and inside the localisation band:

$$\dot{\varepsilon}^o_{kl} = \dot{\varepsilon}_{kl} - \frac{f}{h}(\dot{u}_k n_l)^s = \dot{\varepsilon}_{kl} - \frac{f}{h}\left[C_{ik}{}^{-1}\left(D^o_{ijmn} - D^i_{ijmn}\right)\dot{\varepsilon}_{mn} n_j n_l\right]^s \tag{42}$$

$$\dot{\varepsilon}^i_{kl} = \dot{\varepsilon}_{kl} + \frac{1-f}{h}(\dot{u}_k n_l)^s = \dot{\varepsilon}_{kl} + \frac{1-f}{h}\left[C_{ik}{}^{-1}\left(D^o_{ijmn} - D^i_{ijmn}\right)\dot{\varepsilon}_{mn} n_j n_l\right]^s \tag{43}$$

Therefore, the macro incremental stress-strain relationship can be obtained using (31-33):

$$\dot{\sigma}_{pq} = (1-f)D^o_{pqkl}\dot{\varepsilon}^o_{kl} + fD^i_{pqkl}\dot{\varepsilon}^i_{kl} \tag{44}$$

Substituting (42-43) in the above, and rearranging the obtained expression, we can get the tangent stiffness in the following form:

$$\dot{\sigma}_{pq} = \Bigg[(1-f)D^o_{pqmn} + fD^i_{pqmn} - \frac{f(1-f)}{h}C_{ik}{}^{-1}\left(D^o_{ijmn} - D^i_{ijmn}\right) \times n_j n_l\left(D^o_{pqkl} - D^i_{pqkl}\right)\Bigg]\dot{\varepsilon}_{mn} \tag{45}$$

In the above expression, the first and second terms on the right-hand side represent the upper bound solution of the macro stress increment. The third term accounts for the involvement of the localisation band with orientation $\vec{n}$ and thickness h. For homogeneous deformation, e.g. $D^o_{ijmn} = D^i_{ijmn}$ and $\sigma^i_{ij} = \sigma^o_{ij}$, the above expression automatically collapses to the classical description of a continuum model with tangent stiffness D^i_{ijmn}. In the case of localised failure, the tangent stiffness of the volume element crossed by a localisation band contains mechanical responses of the localisation bands and the region surrounding it, and geometrical properties of both the band (thickness h and orientation $\vec{n}$) and the volume element (its size H, via volume fraction $f = \frac{h}{H}$). This is the key difference with classical continuum models.

As can be seen, the macro incremental response can be obtained given generic incremental responses inside and outside the localisation band (see equations 31-32), the thickness of the band and the effective size of the volume element containing it. In this sense, any existing constitutive models can be enhanced using the proposed two-scale approach to better describe post-localisation behaviour, and only an additional parameter (thickness of the band) is needed. The orientation of the localisation band can be obtained from bifurcation analysis based on the localisation (or acoustic) tensor (see Section 4).

1.3.2. An implicit stress return algorithm

The tangent stiffness (45) can be used for an explicit stress return algorithm. However, given the explicit nature of the process that relies on stress state and internal variables at the previous increment, the internal equilibrium condition (34) will not be met and error will keep accumulating. More importantly, the explicit algorithm is only conditionally stable and hence requires very small strain increments to keep

the error acceptable. Therefore, it is essential to have an implicit iterative algorithm that can accept finite strain increments while always meeting the internal equilibrium condition connecting the stresses inside and outside the localisation zone. Denoting r_i the residual traction vector due to in-equilibrium, we can write:

$$\left(\sigma^o_{ij} - \sigma^i_{ij}\right) n_j = r_i \tag{46}$$

This iterative process starts after an explicit one taking the residual from last step into account. This is considered as zeroth iteration that results in in-equilibrium between tractions inside and outside the localisation band.

Using a first order Taylor expansion of the above equation about a given state, we obtain:

$${r_i}^{new} = {r_i}^{old} + \left(\dot{\sigma}^o_{ij} - \dot{\sigma}^i_{ij}\right) n_j \tag{47}$$

where ${r_i}^{old}$ is the residual traction at this given state. Substituting the generic incremental stress-strain relationships (31-32), and meso-macro strain connections (35-36) in the above expression, we obtain:

$${r_i}^{new} = {r_i}^{old} - D^o_{ijkl}\frac{f}{h}\left(\dot{u}_k n_l\right)^s n_j - D^i_{ijkl}\frac{1-f}{h}\left(\dot{u}_k n_l\right)^s n_j \tag{48}$$

It is noted that this iterative process starts after an explicit one where the macro strain rate $\dot{\varepsilon}_{ij}$ has been applied. As a consequence, $\dot{\varepsilon}_{ij}$ does not appear in the above equation. Enforcing the condition ${r_i}^{new} = 0$ and solving the obtained equation for the velocity jump $\dot{u}_k$, we obtain:

$$\dot{u}_k = {C_{ik}}^{-1} {r_i}^{old} \tag{49}$$

where C_{ik} has been defined in (40). The iterative strain rates $\dot{\varepsilon}^i_{ij}$ and $\dot{\varepsilon}^o_{ij}$ are then:

$$\dot{\varepsilon}^o_{ij} = -\frac{f}{h}\left(\dot{u}_i n_j\right)^s \tag{50}$$

$$\dot{\varepsilon}^i_{ij} = \frac{1-f}{h}\left(\dot{u}_i n_j\right)^s \tag{51}$$

The iterative strain rates $\dot{\varepsilon}^i_{ij}$ and $\dot{\varepsilon}^o_{ij}$ are used for obtaining iterative stress rates $\dot{\sigma}^o_{ij}$, and $\dot{\sigma}^i_{ij}$ and then their total counterparts σ^o_{ij}, and σ^i_{ij}. The iterative process continues until convergence, indicated by a small enough residual r_i compared to the stresses σ^o_{ij}, or σ^i_{ij}. It is worth noticing that the zeroth step can also take any residual from previous steps into account, and due to the enforcement of traction continuity in total form, issues with the accumulation of error do not exist in this implicit algorithm. Given all quantities are continuous functions, the convergence of this Newton-Raphson iterative algorithm depends on how good the first guess is, which in turn is governed by the magnitude of the macro strain increment supplied to the stress return routine. In this sense, sub-incrementation combined with algorithms to return to the last converged state can be used to improve the performance of the stress return routine. Details on the performance of this algorithm can be found in [Nguyen et al., 2016b].

2. A continuum model for inelastic behaviour inside the localisation zone

The damage-plasticity model presented in [Mir, 2017, Mir et al., 2018] is adopted here for both inelastic behaviour inside the localisation band and elastic behaviour outside it. The model has been formulated based on thermodynamics and assessed against experimental data on sandstone failure under triaxial conditions. However, the assessment can only be considered as qualitative given it did not take into account post-localisation behaviour that makes the behaviour of a specimen a BVP (or structural problem). The model will be used in the framework presented above to capture post-localisation behaviour at the constitutive level. In the proposed two-scale approach, this model can be used to provide elastic tangent stiffness D^o_{ijkl} for the behaviour outside the localisation band and inelastic tangent stiffness D^i_{ijkl} for the behaviour inside the localisation band. The formulation of elastic-plastic-damage tangent stiffness D^i_{ijkl} can be found in our earlier publications [Mir, 2017, Mir et al., 2018] and hence is not repeated here. For simplicity in the model descriptions, the superscripts "i" and "o" are dropped and the model is presented as a regular continuum model written for a unit volume element.

2.1. Model descriptions

The model is described using stress invariants in triaxial stress space, with hydrostatic pressure $p = -\sigma_{ii}/3$, shear stress $q = \sqrt{3J_2}$, where $J_2 = \sqrt{\frac{3}{2}s_{ij}s_{ij}}$ is the second invariant of the deviatoric stress tensor $s_{ij} = \sigma_{ij} - \frac{1}{3}\sigma_{kk}\delta_{ij}$. The stress-strain-damage relationships are:

$$p = (1-D)K\varepsilon^e_v = (1-D)K\left(\varepsilon_v - \varepsilon^p_v\right) \tag{52}$$

$$q = 3(1-D)G\varepsilon^e_s = 3(1-D)G\left(\varepsilon_s - \varepsilon^p_s\right) \tag{53}$$

where ε_v and ε_s are volumetric and deviatoric shear strain, with plastic counterparts ε^p_v and ε^p_s, respectively. The bulk and shear moduli are denoted as K, and G, respectively.

The yield function is a function of stress and damage:

$$y = \left(\frac{p-\rho}{\frac{(1-\gamma)p_c - p_t}{(1-D)(p_c+p_t)}p + \frac{\gamma}{2}p_c}\right)^2 + \left(\frac{q-\mu(D)p}{M\left(p - \alpha\sqrt{(1-D)}(p-\rho)\right)}\right)^2 - 1 \leqslant 0 \tag{54}$$

In the above expression M is the slope of the critical state line, attained when $D = 1$; p_t and p_c are isotropic pressures at yield under isotropic tension and compression, respectively; $\mu(D) = D(1-D)\mu_0$ is a function of damage, and ρ is the back stress depending on p_t and p_c:

$$\rho = \frac{(4-\gamma)p_c p_t + \gamma {p_c}^2}{2\left(p_c + p_t\right)} \tag{55}$$

Other parameters of the model are α and γ, which control the shape of the yield surface, and μ_0 that controls the kinematic hardening/softening behaviour [Mir et al., 2018].

The evolution rules for plastic strains and damage are obtained from the yield function y^* written in dissipative stress space, the details of which can be found in [Mir, 2017, Mir et al., 2018]. In true stress space, they are written in pseudo rate forms as:

$$\dot{D} = 2\dot{\lambda}\frac{{r_D}^2\chi_D}{{F_D}^2} \tag{56}$$

$$\dot{\varepsilon}_v^p = 2\dot{\lambda}\left(\frac{{r_v}^2(p-\rho)}{{F_v}^2} - \frac{{r_s}^2\mu(D)\left(q-\mu(D)p\right)}{{F_s}^2}\right) \tag{57}$$

$$\dot{\varepsilon}_s^p = 2\dot{\lambda}\frac{{r_s}^2\left(q-\mu(D)p\right)}{{F_s}^2} \tag{58}$$

where

$$F_v = \frac{1}{r_v}\left(\frac{(1-\gamma)p_c - p_t}{(1-D)\left(p_c+p_t\right)}p + \frac{\gamma}{2}p_c\right) \tag{59}$$

$$F_s = \frac{M}{r_s}\left(p - \beta\sqrt{(1-D)}(p-\rho)\right) \tag{60}$$

$$F_D = \frac{\chi_D}{\sqrt{\left({r_D}^2+{r_s}^2\right)\left(\frac{\chi_v}{r_v F_v}\right)^2 + \left({r_D}^2+{r_v}^2\right)\left(\frac{\chi_s-\mu(D)\chi_v}{r_s F_s}\right)^2}} \tag{61}$$

$$\chi_D = \frac{p^2}{2K(1-D)^2} + \frac{q^2}{6G(1-D)^2} - \rho\frac{\partial\mu}{\partial D}\varepsilon_s^p \tag{62}$$

Parameters r_v, r_s and r_D in the above equations affect the damage-plasticity coupling behaviour of the model and meets the condition ${r_v}^2 + {r_s}^2 + {r_D}^2 = 1$.

2.2. Model behaviour

The model behaviour assessed against two different sandstones with data from [Baud et al., 2004, 2006] is briefly presented in Figs. 4-5, reproduced from our earlier work [Mir, 2017, Mir et al., 2018]. It is noted that all model parameters are calibrated on assumptions that the behaviour is homogeneous, which are incorrect for localised failure observed in tests on these sandstones. The assessment is therefore of qualitative nature only, showing the capability of the model in capturing both brittle and ductile responses of sandstones.

The model parameters used are shown in Table 2, while initial yield surfaces and mechanical behaviour are in Figs. 4 & 5. As can be seen, the model can capture fairly well responses of these sandstones under both low and high confining pressures. However, it is pointless to have a perfect match at this stage without correct underlying failure/deformation mechanism, given the behaviour in these tests is associated with localised failure. This issue will be addressed later using the two-scale approach as an enhancement to this model to describe and capture correctly post-localisation behaviour.

2.3. Rate-dependent regularisation for Finite Element Analysis (FEA)

As addressed, the constitutive behaviour presented above is indicative only, given it is based on an incorrect assumption of homogeneous behaviour. A more rigorous way to perform validation of such models is to use FEA for the solution of BVPs of cylindrical specimens under triaxial loading conditions. For such a purpose, the model presented above is enhanced with rate-dependent behaviour based on Perzyna's type visco-plasticity [Perzyna, 1966]. This is a simple and effective approach that has been adopted in several papers [Das et al., 2013, 2014, Mir, 2017, Mir et al., 2018, Tengattini et al., 2022]. The pseudo rate-dependent behaviour is contained in the constitutive model and there are no inertia effects in the analysis of BVPs. The evolution rules become rate dependent through the multiplier $d\lambda/dt$ such that:

$$d\lambda = \frac{\langle y\rangle}{\eta}dt \tag{63}$$

where η is the viscosity parameter and $\langle y\rangle$ is a dimensionless overstress function derived from the yield function of the rate-independent model, and $\langle . \rangle$ is the Macauley bracket. The evolution rules for plastic strains and damage can be rewritten as:

$$d\varepsilon_v^p = 2\frac{\langle y\rangle}{\eta}\left(\frac{{r_v}^2(p-\rho)}{{F_v}^2} - \frac{{r_s}^2\mu(D)\ \left(q-\mu(D)p\right)}{{F_s}^2}\right)dt \tag{64}$$

$$d\varepsilon_s^p = 2\frac{\langle y\rangle}{\eta}\frac{{r_s}^2\left(q-\mu(D)p\right)}{{F_s}^2}dt \tag{65}$$

$$dD = 2\frac{\langle y\rangle}{\eta}\frac{{r_D}^2\chi_D}{{F_D}^2}dt \tag{66}$$

The behaviour of the rate-dependent model under different rates of axial strain, and values of viscous parameter η is illustrated in Fig. 6, extracted from [Mir et al., 2018].

The FEA results in Fig. 7 show the convergence of the solution with respect to mesh refinement, using parameters for Bentheim sandstone. The axial strain rate $\dot{\varepsilon}_a$ is chosen to be 10^{-5} /s, and viscosity parameter being calibrated as $\eta = 3\times10^{-5}\ s/pa$. Both macro responses of the specimen and failure pattern do not vary significantly upon mesh refinement.

3. Bifurcation and transition from diffuse to localised failure

As seen in Fig. 2, bifurcation of deformation marks the transition from diffuse to localised failure. Beyond the bifurcation point, the behaviour of the specimen under consideration is a BVP requiring enhancements in the structure of constitutive models to describe correctly post-localisation behaviour. This is a topic that has been extensively investigated [Mühlhaus and Vardoulakis, 1987, Neilsen and Schreyer, 1993, Rice and Rudnicki, 1980, Rudnicki and Rice, 1975, Vardoulakis, 1989, Vardoulakis et al., 1978, Vardoulakis and Sulem, 1995]. It is important to note that classical constitutive models are not valid beyond the bifurcation point unless they are enhanced to handle post-localisation behaviour. Our proposed two-scale constitutive modelling approach is an example of such enhancements that allows correctly capturing both pre- and post-localisation behaviour. Therefore, the determination of bifurcation point is an essential and important part of the approach presented above, and this Section briefly presents how to determine bifurcation points for the transition from diffuse to localised failure in constitutive modelling.

The bifurcation condition based on the loss of positive-definiteness of the acoustic tensor (or localisation tensor)

Table 2. Model parameters for Bentheim and Darley Dale sandstones [Mir, 2017, Mir et al., 2018].

Sandstone	E (GPa)	ν	β	γ	μ_0	M	p_c (MPa)	p_t (MPa)	r_v	r_s
Bentheim [Baud et al., 2006]	19.25	0.27	0.85	0.95	0.10	1.20	420.00	-12.00	0.85	0.20
Berea [Baud et al., 2004]	14.00	0.20	0.90	1.00	0.05	1.10	380.00	-10.00	0.85	0.20

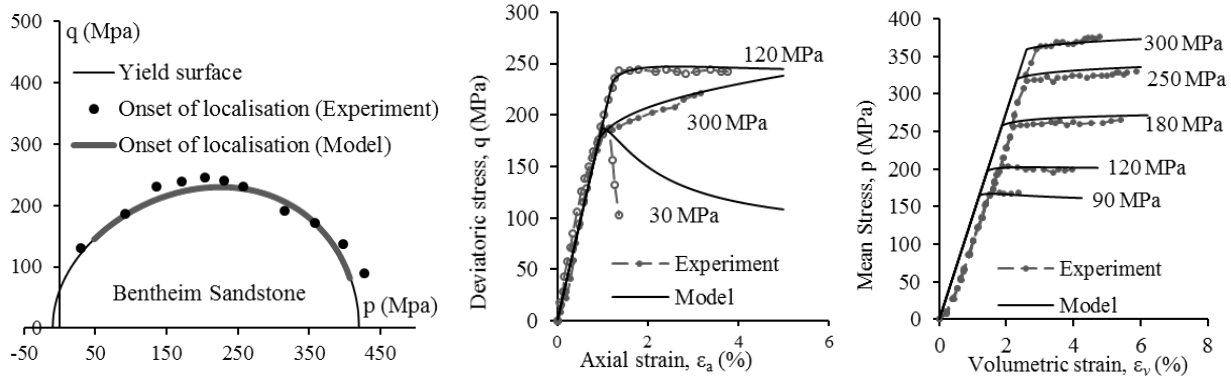

(a) Initial yield surface.

(b) Behaviour.

Figure 4. Constitutive behaviour of Bentheim sandstone [Mir et al., 2018].

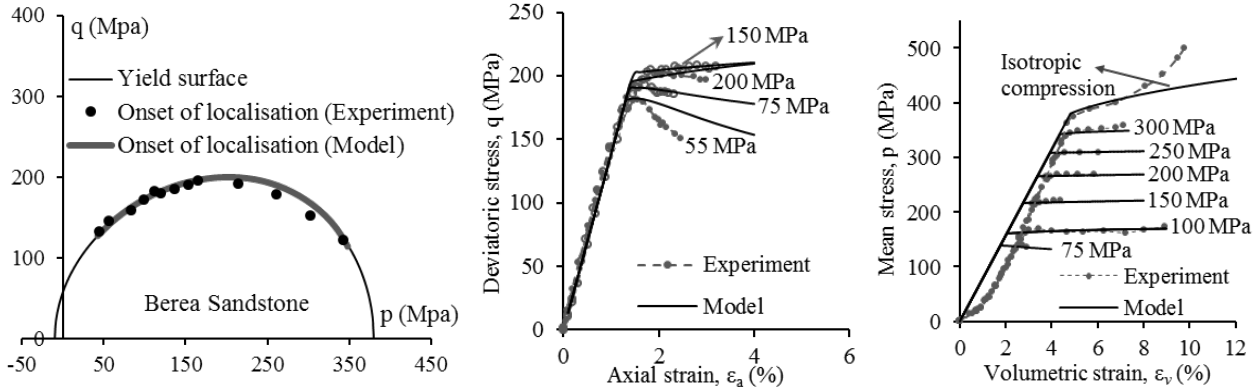

(a) Initial yield surface.

(b) Behaviour.

Figure 5. Constitutive behaviour of Berea sandstone [Mir et al., 2018].

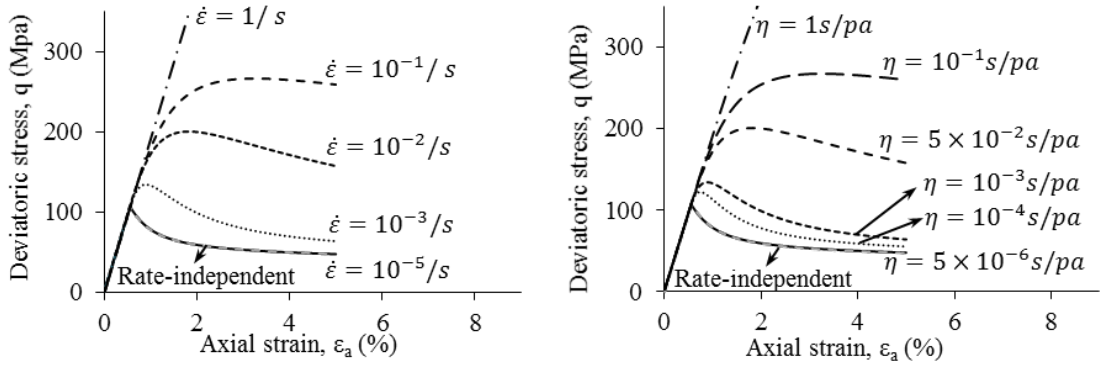

(a) Effect of strain rate (η 5×10^{-6} s/pa).

(b) Effect of viscosity parameter (Ω $10^{-5}/s$).

Figure 6. Rate-dependent behaviour in triaxial loading under 10MPa confining pressure (E = 20 GPa, ν = 0.27, p_c = 420 MPa, p_t = -12 MPa, M = 1.2, β = 0.85, γ = 0.95, μ_0 = 0.1, r_v = 0.85 and r_s = 0.2).

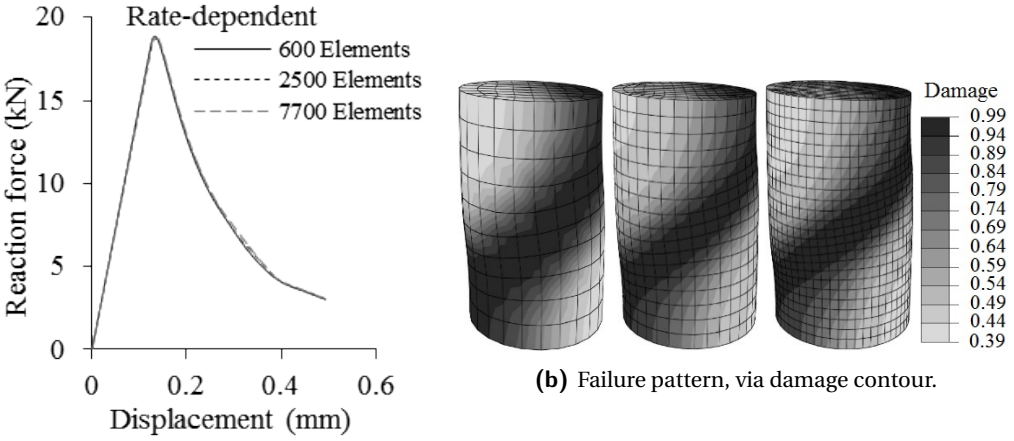

(a) Convergence of FEA results.

(b) Failure pattern, via damage contour.

Figure 7. Rate-dependent behaviour in FEA of a cylindrical specimen under 10MPa confining pressure [Mir et al., 2018].

proposed by [Rudnicki and Rice, 1975] has been widely used in the literature to detect bifurcation point of constitutive behaviour. Recalling the relationship (38) rewritten in incremental form:

$$\left(D^o_{ijkl} - D^i_{ijkl}\right)\delta\varepsilon_{kl} n_j - \left[\frac{f}{h} D^o_{ijkl} n_l n_j + \frac{1-f}{h} D^i_{ijkl} n_l n_j\right]\delta u_k = 0 \quad (67)$$

It is usually assumed that the strain increment $\delta\varepsilon_{kl}$ is constrained to evolve continuously [Neilsen and Schreyer, 1993], and under such conditions the tangent moduli D^o_{ijkl} and D^i_{ijkl} coincide at the onset of localisation. We do not go into a debate here about the validity of such an assumption which is questionable for elasto-plastic models with discontinuity of tangent modulus at yield point (elasto-plastic stiffness for loading, and elastic stiffness for unloading), the resolution of which requires further developments beyond the scope of this paper. Instead, the practical aspect of such an assumption that allows a rather straightforward way to detect the onset of localisation is addressed. Under the assumption that $D^o_{ijkl} = D^i_{ijkl}$, the above equation becomes:

$$\frac{1}{h}\left(D^i_{ijkl} n_l n_j\right)\delta u_k = 0 \quad (68)$$

For non-trivial solutions (e.g. $\delta u_k \neq 0$), it is required that:

$$\det\left(\frac{1}{h} D^i_{ijkl} n_l n_j\right) = \det\left(\frac{1}{h} A_{ik}\right) = 0 \quad (69)$$

where A_{ik} is the localisation tensor and $\frac{1}{h}A_{ik}$ has the physical meaning of stiffness of a localisation band of thickness h and orientation defined by normal vector $\vec{n}$. For elasto-plastic models with discontinuous tangent modulus at the onset of yielding, the determinant of the localisation tensor also exhibits a jump from positive to negative values corresponding to the switch from elastic to elasto-plastic behaviour. Given the physical meaning of $\frac{1}{h}A_{ik}$, the minimum value of $\det\left(\frac{1}{h}A_{ik}\right)$ with respect to normal vector $\vec{n}$ can be used to determine the orientation of the localisation band. This condition, written as

$$\min_{\vec{n}} \left[\det\left(A_{ik}\right)\right] \leqslant 0 \quad (70)$$

has been applied to different models for soils, soft and hard rocks for the determination of both onset of localisation and orientation of the localisation band, with some results obtained having been validated against experimental data. The readers can also refer to our earlier papers [Le et al., 2020, 2019] for the application of such condition for cohesive-frictional models representing the behaviour of a localisation band of infinitesimal thickness. Figure 8 below is an illustration of the onset of compaction localisation determined under triaxial condition using a model based on breakage mechanics [Nguyen et al., 2016a].

Stress states on the initial yield envelope are used for localisation condition (69) and the results are highlighted in red, with corresponding localisation angles indicated in Fig. 8a. The zone with negative determinant of the determinant of the acoustic tensor is indicated in Fig. 8b, along with contour of this determinant plotted against the band orientation angle and normalised mean stress ($\frac{p}{P_{cr}}$, with P_{cr} the pressure at yield under hydrostatic loading condition). As can be seen in Fig. 8b, for a given stress state there is a range of inclination angles that are admissible for bifurcation condition using (69) and the minimum value of the determinant of the localisation tensor can be used to determine the orientation of the localisation band.

For both hard and soft rocks, depending on the focus on different modes of localised failure, different models based on breakage mechanics [Das et al., 2011, 2014] and damage mechanics [Mir, 2017, Mir et al., 2018], all coupled with plasticity, have been developed and used with success. Figure 9 presents the results on bifurcation obtained from a damage-plasticity model for soft rocks described in Section 3 [Mir, 2017, Mir et al., 2018]. The blue thick line on the initial yield surface in this figure indicates the stress states at which bifurcation of deformation initiates. Three triaxial loading paths in this figure at 10 MPa, 120 MPa and 250 MPa confining pressures are illustrated and their intersections

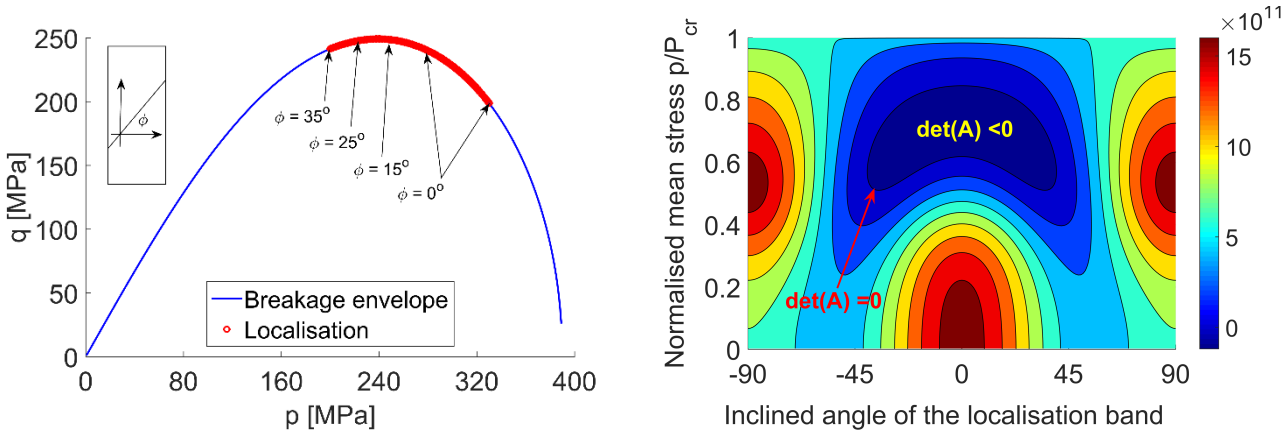

(a) Predicted zone of localisation.

(b) Contour of the determinant of the acoustic tensor.

Figure 8. Onset of localisation and orientation of localisation band determined under triaxial condition using a model based on breakage mechanics [Nguyen et al., 2016b].

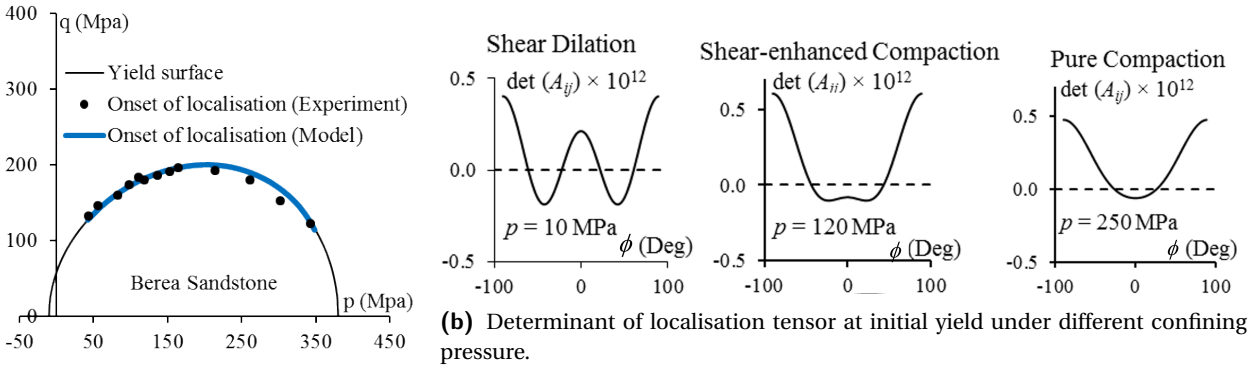

(a) Onset of localisation.

(b) Determinant of localisation tensor at initial yield under different confining pressure.

Figure 9. Onset of localisation in Berea sandstone determined under triaxial condition using a coupled damage-plasticity model.

with the initial yield surface provide stress states for the determination of onset of bifurcation using equation (69). For each stress state, determinant of the localisation tensor is plotted against angle of potential localisation band (with respect to the horizontal). The shape of the curve gradually transforms and reflects the transformation of localised failure modes: from shear localisation at low confining pressure, which results in two inclined angles due to symmetry in triaxial tests, to compaction localisation with a single horizontal compaction band at sufficiently high confining pressures. The theoretical results are consistent with the experimental observation of shear-enhanced compaction localisation in sandstones [Baud et al., 2004].

Similar results have also been obtained using a damage-plasticity model for hard rocks [Mir, 2017]. The transformation of the curve in Fig. 10 also reflects the transition from shear localisation to compaction localisation in triaxial loading conditions with increasing confining pressure. The model's predictions are also included for illustration purpose, although it is clear that the post-peak prediction is not meaningful due to localisation, making the problem a BVP that cannot be handled by a classical constitutive model. Behaviour of the model described in Section 3 after being enhanced with an embedded localisation band using our proposed two-scale constitutive modelling approach will be illustrated in the next Section.

4. Analysis of localised failure

The damage-plasticity model described in Section 3 is used for the analysis of localised failure in two different ways. Its rate-dependent enhancement, presented in Section 3, will be used in FEA to provide insights into local responses in the specimen (inside and outside localisation band) that follow different loading paths due to localisation. The enhancement at the constitutive level using the proposed thermodynamics-based two-scale approach allows describing and capturing correctly post-localisation behaviour at the constitutive level. In other words, the proposed two-scale approach enriches existing constitutive models with size dependent behaviour required to deal with localised failure and hence post-localisation behaviour can be correctly described and captured at the constitutive level. This is of course a simplification of a much more complex BVP so that localised failure can be tackled in a simplest possible but physically meaningful way at the constitutive level.

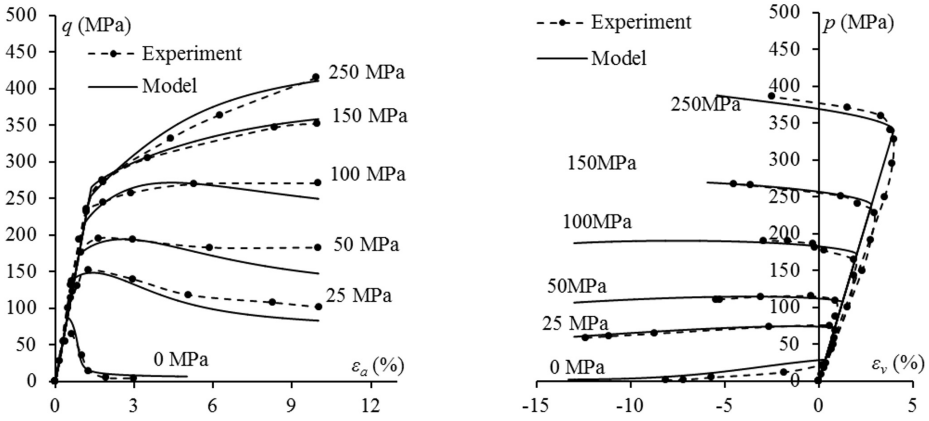

(a) Stress-strain behaviour (left) and volumetric responses (right).

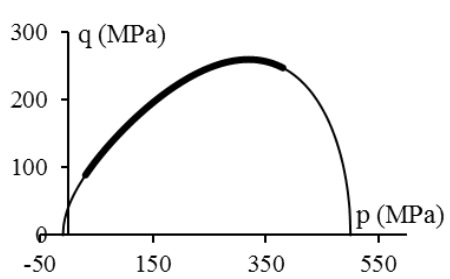

(b) Onset of localisation.

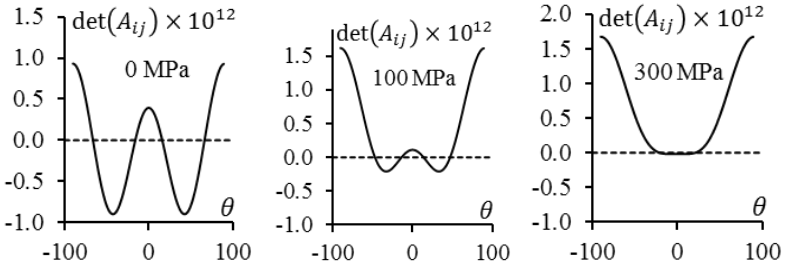

(c) Determinant of localisation tensor at initial yield under different confining pressure.

Figure 10. Onset of localisation (grey thick line) in Ural marble at different stress states at initial yield under triaxial loading [Mir, 2017].

The benefits include (i) physically meaningful correlation between behaviour and failure mode in constitutive modelling that helps minimise the use of fitting parameters [Le et al., 2018, 2019, 2017], (ii) good balance between computational efficiency and accuracy of the prediction [Nguyen et al., 2017, Nguyen and Bui, 2020, Nguyen et al., 2016b], and (iii) explicit links between meso-scale behaviour of the localisation band and macro (specimen) behaviour that are useful for the determination of behaviour inside the localisation band from standard triaxial tests [Le et al., 2022]. The readers can refer to our papers on the use of this two-scale approach in FEM, MPM and SPH applications [Bui and Nguyen, 2021, Le et al., 2018, 2019, Nguyen and Bui, 2020, Nguyen et al., 2014, 2016b, Tran et al., 2019, Wang et al., 2019, 2020]. The analysis of localised failure in this Section illustrates the performance of the model against detailed FEM modelling of a triaxial test. This assessment, focusing on a sandstone under triaxial loading condition and the mechanism of localized failure that a constitutive model should possess to describe correctly both pre- and post-localisation behaviour, has not been included in our earlier publications listed above.

4.1. Calibration of model parameters

The behaviour and thickness of localisation band evolve together and ideally these evolutions should be considered in constitutive modelling and calibration of model parameters. However, once localized failure happens the problem will become a BVP and hence modelling the evolutions of the band thickness and material behaviour inside the band requires solving a BVP. That approach is usually complicated given it needs a regularisation technique to deal with ill-posed BVPs due to localised failure and also complex procedures to calibrate two sets of parameters (a length scale, and parameters of the constitutive model; see [Nguyen and Houlsby, 2007]), subjected to several constraints (macro specimen response, meso-scale responses including evolutions of localisation band and its behaviour). In addition, there are no explicit links between experimental data and these parameters, making the identification and calibration of parameters complicated, especially with the analysis of a BVP needed for the calibration.

The approach proposed in this paper is a simplification of physical observations briefly discussed above, in the sense that the thickness of the band is fixed. The proposed approach and derived models contain two set of parameters: thickness of the localisation band, and parameters governing the behaviour inside this band. Therefore, the calibration of model parameters is different from that of classical continuum models (based on assumed homogeneous deformation). In this paper, a simple calibration approach is used for illustration purpose only, in which the determination of the band thickness and calibration of parameters governing the mechanical behaviour of the localisation band are not coupled. Parameters of the constitutive model can be calibrated so that the onset of localisation and orientation of localisation band are close to experimental counterparts, beside being able to reproduce

the trend of macro mechanical responses of the specimens. The thickness of the band will then be used to obtain good fit with experimentally measured mechanical responses. This procedure is obviously an ad hoc process to achieve good fit based on an extra length scale, given the two sets of parameters controlling the continuum behaviour and thickness of localisation band should correlate with each other, as shown in our previous work on nonlocal approaches [Nguyen and Houlsby, 2007].

In general, for the two-scale approach proposed in this paper, the calibration of model parameters must be accompanied with a procedure to analyse results of triaxial tests involving localised failure. This is because besides the macro responses, both orientation and thickness of the localisation band produced by the model must match their experimental counterparts. This requires more experimental data than usual: both macro responses and meso-scale details must be supplied, and this is not always the case in standard triaxial tests. It can be assumed that the orientation of localisation band can be supplied, as this is straightforward and does not require complicated procedures or instrumentations. The thickness h can be assumed based on mean grain size (or aggregate size in concrete), or from analysis of experimental data if advanced image based instrumentations (DIC, X-ray) are available (see examples in [Andò, 2013, Andò et al., 2013, Rattez et al., 2022]). It is noted that the fixed value of band thickness is a strong approximation and to the best of our knowledge there is no consensus in determining it given this assumption does not reflect well experimental observations (evolving thickness). From the assumed value of thickness, the links between meso behaviour inside the band and macro experimental data can be used to obtain behaviour inside the band. This meso scale behaviour should be used for the calibration of model parameters. Details on this approach to analysing experimental data involving localised failure has been elaborated and illustrated in [Le et al., 2022]. This analysis of experimental data should be coupled with calibration procedures to obtain a good match between experiment and modelling in both pre- and post-localisation stages, including the onset and orientation of localisation band. Such a more rigorous approach needs more time for investigation and hence cannot be covered in this paper.

4.2. Results and analysis

Figure 11a shows the results of the FEA simulation of a Bentheim sandstone specimen under drained triaxial test at 30 MPa confining pressure. In this FEA simulation, a local defect is introduced as a weak element at about the centre of each specimen to trigger localisation. The overall stress-strain response of the specimen is calculated as the average of the stress-strain responses of the material inside and outside the band. Responses of two elements inside and outside the localisation band are also plotted, showing different loading paths: elastic unloading outside the band, and inelastic loading inside it. It is clear from this figure that such a behaviour of a BVP cannot be correctly described by a classical continuum constitutive model that is formulated based on the assumption of homogeneity. In this sense, any attempt, without resorting to the underlying mechanisms of failure, to obtain a good match with the post-localisation macro responses of the specimen is merely a curve fitting exercise, at least in our opinion.

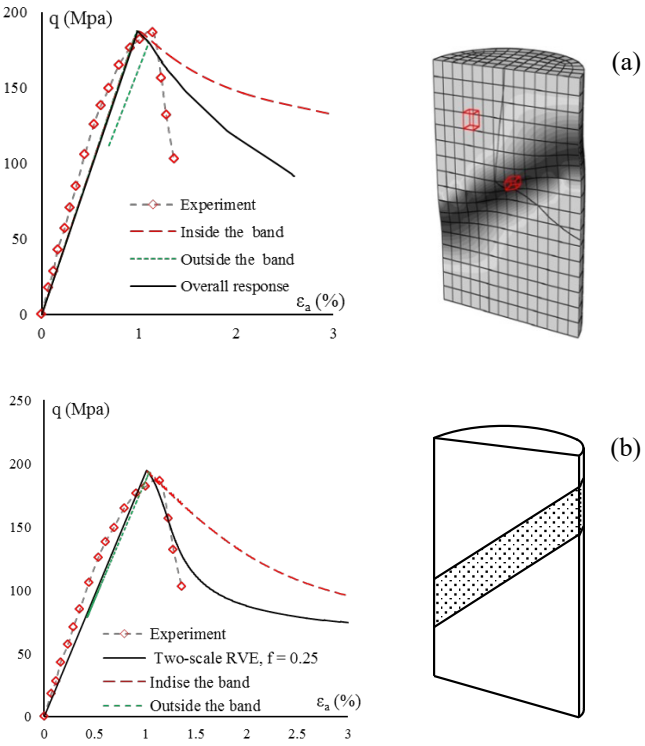

Figure 11. Average stress-strain responses for the material inside and outside the localisation band for a specimen of Bentheim sandstone under 30 MPa confining pressure: (a) FE simulation. (b) The two-scale model with $f = h/H = 0.25$ [Mir, 2017].

The enhancement to the model presented in Section 3.1, based on two-scale constitutive approach, can reproduce the same trend of behaviour at a fraction of the computational cost compared to FEA (Fig. 11b). In particular the time to complete the calculations at the material point level (using our FORTRAN code) is within a minute, while FEA time (using ABAQUS and UMAT routine) is at the order of a few hours. In this sense the difference is clearly at least 2 orders of magnitudes (~1 minute vs. minimum 2-5 hours, depending the FE mesh and model, and also number of CPU cores used). It is noted that the specimen and shear band drawn in Fig. 11b, based on the angle obtained from the analysis of the onset of localisation (Section 5), is for illustrative purpose only, given all these details appear as parameters of the two-scale constitutive model. The enhancement using the proposed two-scale approach allows two different responses inside and outside the localisation band, the combination of which reproduces the experimentally-observed behaviour. The model behaviour in this case is governed by the underlying mechanism of failure (shear localisation, with failure mode indicated in Fig. 11b) and not based on curve fitting model responses with experimental data as usually the case in classical continuum models.

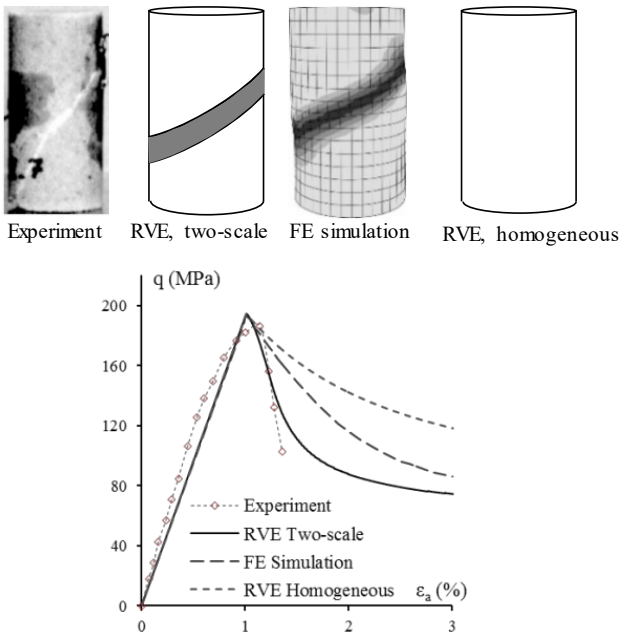

Figure 12. Behaviour and failure mode of a specimen of Bentheim sandstone under 30 MPa confining pressure [Mir, 2017].

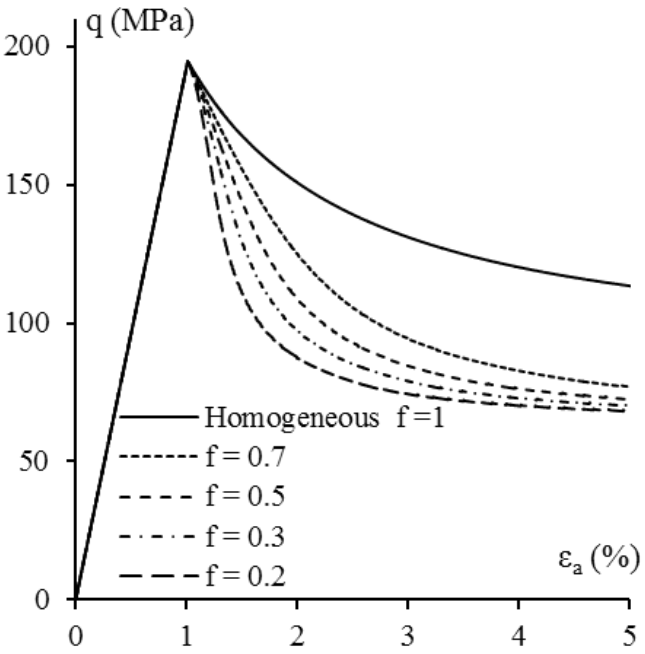

Figure 13. The effect of the width of the localisation band on the average stress-strain response of a specimen modelled by means of the two-scale model [Mir, 2017].

For illustration, the results from three different approaches that are based on the same damage-plasticity model described in Section 3 are shown in Fig. 12, along with the underling failure mode and experimental counterparts. The key point in the figure is the correlation between the underlying failure mode and macro behaviour which is missing in classical continuum models given such models are formulated based on an incorrect assumption of homogeneous distribution of stress and strain in a RVE. Of course, classical continuum models can be fine-tuned to fit the experimental results. However, a good match with experimental result without being based on a correct mechanism of failure is physically meaningless, as such a match is purely curve fitting. It is therefore stressed here that the mechanism of failure (or failure mode) should be focussed on first in constitutive modelling of geomaterials, before attempting the fine-tuning process for calibration of model parameters and validation with experimental data. In this sense, the proposed structure of the two-scale model and the prediction of orientation of localisation band are the first steps that are then followed by tuning other parameters. In the above example, our volume fraction $f = h/H = 0.25$ used in the two-scale approach is obtained for a good fit with experimental data, using parameters of the damage-plasticity model presented in Section 3.

The effect of thickness of localisation band on constitutive response is illustrated in Fig. 13. This is the size effect behaviour given the specimen response scales with the ratio between thickness of the band and the size of the volume element containing the band. For comparison purpose, the thickness of the localisation band can be fine tuned so that the overall response produced by the two-scale model can match that by FEA using the same core damage-plasticity model enhanced with rate-dependent regularisation. Both macro response and variation of kinematic fields across the localisation band obtained using the two-scale model and FEA can be assessed against each other (Fig. 14).

The two-scale model assumes the width of the localisation band to be invariant throughout post-localisation phase of deformation. This assumption approximates the variations of the kinematic field within the localisation band and the surrounding bulk and can help reduce the computational cost significantly given the whole BVP analysed using FEA can be approximated with reasonable accuracy but at a fraction of the computational cost. It is noted that the FEA based on the rate-dependent regularised model above (or alternatively non-local and gradient models) can definitely produce much better gradual variation of the kinematic fields across the localisation band. However, the implementation and application of these models require a discretisation size smaller than the width of the localisation band. If the location of the band is also unknown, then the whole domain under consideration should be discretised with the spatial resolution smaller than the bandwidth. This would severely limit the applications of high order models in very large-scale problems of geotechnical and mining engineering. The two-scale model approximates the variation of the displacement and strain fields by assuming a constant bandwidth h and uniform distribution of stress and strain inside the localisation band. This bandwidth is then directly incorporated in the constitutive equations and the interaction between the materials inside and outside the band at the constitutive level. Therefore, the application of the two-scale approach and models does not require element size smaller than the bandwidth, but in fact the opposite:

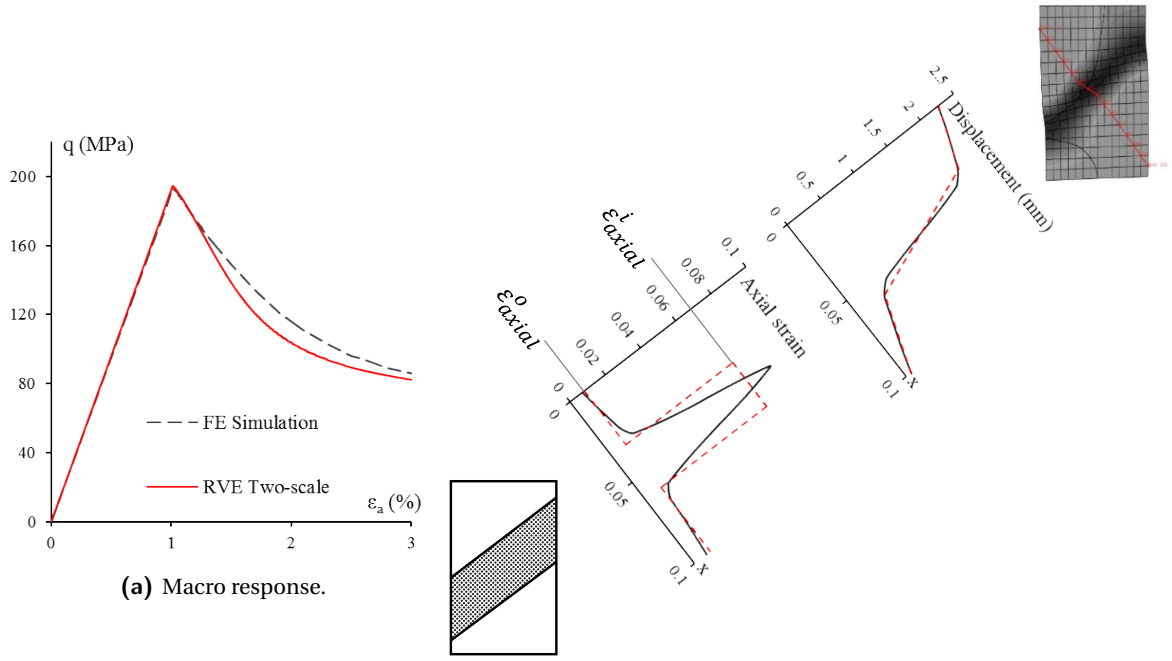

(a) Macro response.

(b) Strain and displacement profile across the localisation band at late stage of the failure process.

Figure 14. Two-scale approach vs. FEA.

the element size (or particle size) should be larger than the thickness of the localisation band contained in it. This feature of the two-scale model makes it desirable for large-scale modelling in geotechnical and mining engineering. However, for smaller scale problems, models regularised using rate-dependent, nonlocal or gradient theories combined with FEA produce more accurate results, although at significantly higher computational costs.

Nevertheless, assuming a constant width for the localisation band poses some challenges in selecting the bandwidth h as an input parameter for the two-scale approach. A common strategy for measuring the length scale either in modelling or experiments [Rattez et al., 2022] is to use the profile of strain across the localisation band. The main question is, therefore, how the length scale h and variation of constitutive behaviour can be quantified across the localisation band. Providing an answer to this question, however, requires further experimental and numerical investigations at the grain scale, all of which are outside the scope of this study. Along this line, an attempt has been made to idealise the evolution of the localisation band as a zone of uniform distribution of deformation but with thickness evolving [Nguyen and Bui, 2020]. This can be a basis for further developments.

5. Conclusions

We have shown the benefits of adding the behaviour of another scale below the macro RVE scale to a constitutive model. The proposed two-scale constitutive modelling approach can be formulated thermodynamically consistently, and can be used to enhance a classical continuum model to describe correctly post-localisation behaviour at the constitutive level. In principle, any available continuum model can be used in the proposed two-scale approach. Only an extra parameter related to the thickness of the localisation band is needed, and the orientation of the band can be predicted using the employed continuum constitutive model. We stress on the underlying mechanism of localised failure as a prerequisite in constitutive modelling of geomaterials that should be incorporated in the structure of constitutive model before attempting to calibrate model parameters and perform validation. In this sense, a good match with experimental data is only physically meaningful if is accompanied by a correct underlying mechanism of failure. The examples and results provided are to illustrate key features of the proposed two-scale constitutive modelling approach. As can be seen they do not provide excellent match with experimental data as it is not the purpose of the illustration. Instead, our discussions are on the physically meaningful aspects of the approach given there are still several unsolved issues to improve the consistency and correctness of the proposed approach for better matches with experimental results. They will be addressed in our future work.

Conflicts of Interest

The authors declare no conflicts of interest. The complete review history is available online.

Acknowledgements

The authors gratefully acknowledge support from the Australian Research Council via Discovery Projects FT140100408

(Nguyen), DP170103793 (Nguyen & Bui), DP190102779 (Bui & Nguyen), and FT200100884 (Bui).

References

Alshibli, K. A. and Hasan, A. (2008). Spatial variation of void ratio and shear band thickness in sand using X-ray computed tomography. *Géotechnique*, 58(4):249–257.

Andò, E. (2013). *Experimental Investigation of Microstructural Changes in Deforming Granular Media Using x-Ray Tomography*. PhD thesis, Université de Grenoble.

Andò, E., Viggiani, G., Hall Stephen, A., and Desrues, J. (2013). Experimental micro-mechanics of granular media studied by x-ray tomography: Recent results and challenges. *Géotechnique Letters*, 3(3):142–146.

Baud, P., Klein, E., and Wong, T.-f. (2004). Compaction localization in porous sandstones: Spatial evolution of damage and acoustic emission activity. *Journal of Structural Geology*, 26(4):603–624.

Baud, P., Vajdova, V., and Wong, T.-F. (2006). Shear-enhanced compaction and strain localization: Inelastic deformation and constitutive modeling of four porous sandstones. *Journal of Geophysical Research (Solid Earth)*, 111.

Bažant, Z. P. (1991). Why Continuum Damage is Nonlocal: Micromechanics Arguments. *Journal of Engineering Mechanics*, 117(5):1070–1087.

Borja, R. I. (2000). A finite element model for strain localization analysis of strongly discontinuous fields based on standard Galerkin approximation. *Computer Methods in Applied Mechanics and Engineering*, 190(11–12):1529–1549.

Bui, H. H. and Nguyen, G. D. (2021). Smoothed particle hydrodynamics (SPH) and its applications in geomechanics: From solid fracture to granular behaviour and multiphase flows in porous media. *Computers and Geotechnics*, 138.

Charalampidou, E.-M., Hall, S. A., Stanchits, S., Viggiani, G., and Lewis, H. (2014). Shear-enhanced compaction band identification at the laboratory scale using acoustic and full-field methods. *International Journal of Rock Mechanics and Mining Sciences*, 67:240–252.

Chemenda, A. I. (2011). Origin of compaction bands: Anti-cracking or constitutive instability? *Tectonophysics*, 499(1):156–164.

Chen, Z. and Schreyer, H. L. (1987). Simulation of Soil-Concrete Interfaces with Nonlocal Constitutive Models. *Journal of Engineering Mechanics*, 113(11):1665–1677.

Das, A., Nguyen, G., and Einav, I. (2011). Compaction bands due to grain crushing in porous rocks: A theoretical approach based on breakage mechanics. *Journal of Geophysical Research: Solid Earth*, 116.

Das, A., Nguyen, G., and Einav, I. (2013). The propagation of compaction bands in porous rocks based on breakage mechanics. *Journal of Geophysical Research: Solid Earth*, 118:2049–2066.

Das, A., Tengattini, A., Nguyen, G. D., Viggiani, G., Hall, S. A., and Einav, I. (2014). A thermomechanical constitutive model for cemented granular materials with quantifiable internal variables. Part II – Validation and localization analysis. *Journal of the Mechanics and Physics of Solids*, 70:382–405.

De Borst, R. and Mühlhaus, H.-B. (1992). Gradient-dependent plasticity: Formulation and algorithmic aspects. *International Journal for Numerical Methods in Engineering*, 35(3):521–539.

Einav, I. (2007a). Breakage mechanics–Part I: Theory. *Journal of the Mechanics and Physics of Solids*, 55(6):1274–1297.

Einav, I. (2007b). Breakage mechanics–Part II: Modelling granular materials. *Journal of the Mechanics and Physics of Solids*, 55(6):1298–1320.

Houlsby, G. T. and Puzrin, A. M. (2000). A thermomechanical framework for constitutive models for rate-independent dissipative materials. *International Journal of Plasticity*, 16(9):117–1047.

Houlsby, G. T. and Puzrin, A. M. (2006). *Principles of Hyperplasticity - An Approach to Plasticity Theory Based on Thermodynamic Principles*. Springer-Verlag, London.

Jirásek, M. (1998). Nonlocal models for damage and fracture: Comparison of approaches. *International Journal of Solids and Structures*, 35(31–32).

Jirásek, M. (2000). Comparative study on finite elements with embedded discontinuities. *Computer Methods in Applied Mechanics and Engineering*, 188(1):307–330.

Larsson, R., Runesson, K., and Sture, S. (1996). Embedded localization band in undrained soil based on regularized strong discontinuity–theory and FE-analysis. *International Journal of Solids and Structures*, 33(20–22):3081–3101.

Le, L. A., Nguyen, G. D., and Bui, H. H. (2020). Predicting onset and orientation of localisation bands using a cohesive-frictional model. In Ha-Minh, C., Dao, D. V., Benboudjema, F., Derrible, S., Huynh, D. V. K., and Tang, A. M., editors, *CIGOS 2019, Innovation for Sustainable Infrastructure*, pages 311–316, Singapore. Springer Singapore.

Le, L. A., Nguyen, G. D., Bui, H. H., and Andrade, J. E. (2022). Localised failure of geomaterials: how to extract localisation band behaviour from macro test data. *Géotechnique*, 72(7):596–609.

Le, L. A., Nguyen, G. D., Bui, H. H., Sheikh, A. H., and Kotousov, A. (2018). Localised failure mechanism as the basis for constitutive modelling of geomaterials. *International Journal of Engineering Science*, 133:284–310.

Le, L. A., Nguyen, G. D., Bui, H. H., Sheikh, A. H., and Kotousov, A. (2019). Incorporation of micro-cracking and fibre bridging mechanisms in constitutive modelling of fibre reinforced concrete. *Journal of the Mechanics and Physics of Solids*, 133.

Le, L. A., Nguyen, G. D., Bui, H. H., Sheikh, A. H., Kotousov, A., and Khanna, A. (2017). Modelling jointed rock mass as a continuum with an embedded cohesive-frictional model. *Engineering Geology*, 228:107–120.

Lubarda, V. A. and Krajcinovic, D. (1993). Damage tensors and the crack density distribution. *International Journal of Solids and Structures*, 30(20):2859–2877.

Mir, A. (2017). *A Thermodynamic Approach to Modelling Brittle-Ductile and Localised Failure of Rocks Using Damage Mechanics and Plasticity Theory*. PhD thesis, University of Adelaide, Adelaide.

Mir, A., Nguyen, G. D., and Sheikh, A. H. (2018). A thermodynamics-based model for brittle to ductile behaviour and localised failure of porous rocks. *International Journal of Solids and Structures*, 152:161–184.

Mollema, P. N. and Antonellini, M. A. (1996). Compaction bands: A structural analog for anti-mode I cracks in aeolian sandstone. *Tectonophysics*, 267(1):209–228.

Mühlhaus, H. B. and Vardoulakis, I. (1987). The thickness of shear bands in granular materials. *Géotechnique*, 37(3):271–283.

Neilsen, M. K. and Schreyer, H. L. (1993). Bifurcations in elastic-plastic materials. *International Journal of Solids and Structures*, 30(4):521–544.

Nguyen, C. T., Nguyen, G. D., Das, A., and Bui, H. H. (2017). Constitutive modelling of progressive localised failure in porous sandstones under shearing at high confining pressures. *International Journal of Rock Mechanics and Mining Sciences*, 93:179–195.

Nguyen, G. and Houlsby, G. (2007). Non-local damage modelling of concrete: A procedure for the determination of model parameters. *International Journal for Numerical and Analytical Methods in Geomechanics*, 31(7):687–891.

Nguyen, G. D. and Bui, H. H. (2020). A thermodynamics- and mechanism-based framework for constitutive models with evolving thickness of localisation band. *International Journal of Solids and Structures*, 187:100–120.

Nguyen, G. D., Einav, I., and Korsunsky, A. M. (2012). How to connect two scales of behaviour in constitutive modelling of geomaterials. *Géotechnique Letters*, 2(3):129–134.

Nguyen, G. D., Korsunsky, A. M., and Einav, I. (2014). A constitutive modelling framework featuring two scales of behaviour: Fundamentals and applications to quasi-brittle failure. *Engineering Fracture Mechanics*, 115:221–240.

Nguyen, G. D., Nguyen, C. T., Bui, H. H., and Nguyen, V. P. (2016a). Constitutive modelling of compaction localisation in porous sandstones. *International Journal of Rock Mechanics and Mining Sciences*, 83:57–72.

Nguyen, G. D., Nguyen, C. T., Nguyen, V. P., Bui, H. H., and Shen, L. (2016b). A size-dependent constitutive modelling framework for localised failure analysis. *Computational Mechanics*, 58(2):257–280.

Oliver, J. (1996). Modelling Strong Discontinuities in Solid Mechanics Via Strain Softening Constitutive Equations. Part 1: Fundamentals. *International Journal for Numerical Methods in Engineering*, 39(21):3575–3600.

Oliver, J., Huespe, A. E., and Sánchez, P. J. (2006). A comparative study on finite elements for capturing strong discontinuities: E-FEM vs X-FEM. *Computer Methods in Applied Mechanics and Engineering*, 195(37):4732–4752.

Perzyna, P. (1966). Fundamental problems in viscoplasticity. *Advances in Applied Mechanics*, 9:243–377.

Pietruszczak, S. (1999). On Homogeneous and Localized Deformation in Water-Infiltrated Soils. *International Journal of Damage Mechanics*, 8(3):233–253.

Pietruszczak, S. and Haghighat, E. (2015). Modeling of deformation and localized failure in anisotropic rocks. *International Journal of Solids and Structures*, 67-68:93–101.

Pietruszczak, S. and Mróz, Z. (1981). Finite element analysis of deformation of strain-softening materials. *International Journal for Numerical Methods in Engineering*, 17(3):327–334.

Pietruszczak, S. and Mroz, Z. (2001). On failure criteria for anisotropic cohesive-frictional materials. *International Journal for Numerical and Analytical Methods in Geomechanics*, 25(5):509–524.

Pietruszczak, S. and Xu, G. (1995). Brittle response of concrete as a localization problem. *International Journal of Solids and Structures*, 32(11):1517–1533.

Pijaudier-Cabot, G. and Bažant, Z. P. (1987). Nonlocal damage theory. *Journal of Engineering Mechanics*, 113(10):1517–1533.

Pour, A. F., Verma, R. K., Nguyen, G. D., and Bui, H. H. (2022). Analysis of transition from diffuse to localized failure in sandstone and concrete using Digital Image correlation. *Engineering Fracture Mechanics*, 267.

Rattez, H., Shi, Y., Sac-Morane, A., Klaeyle, T., Mielniczuk, B., and Veveakis, M. (2022). Effect of grain size distribution on the shear band thickness evolution in sand. *Géotechnique*, 72(4).

Rice, J. R. and Rudnicki, J. W. (1980). A Note on Some Features of the Theory of Localization of Deformation. *International Journal of Solids and Structures*, 16(7):597–605.

Rudnicki, J. W. and Rice, J. R. (1975). Conditions for the localization of deformation in pressure-sensitive dilatant materials. *Journal of the Mechanics and Physics of Solids*, 23(6):371–394.

Samaniego, E. and Belytschko, T. (2005). Continuum–discontinuum modelling of shear bands. *International Journal for Numerical Methods in Engineering*, 62(13):1857–1872.

Sanborn, S. E. and Prévost, J. H. (2011). Frictional slip plane growth by localization detection and the extended finite element method (XFEM). *International Journal for Numerical and Analytical Methods in Geomechanics*, 35(11):1278–1298.

Sternlof, K. R., Rudnicki, J. W., and Pollard, D. D. (2005). Anticrack inclusion model for compaction bands in sandstone. *Journal of Geophysical Research: Solid Earth*, 110(B11).

Tengattini, A., Nguyen, G. D., Viggiani, G., and Einav, I. (2022). Micromechanically inspired investigation of cemented granular materials: Part II– from experiments to modelling and back. *Acta Geotechnica*.

Thakur, V., Nordal, S., Viggiani, G., and Charrier, P. (2017). Shear bands in undrained plane strain compression of Norwegian quick clays. *Canadian Geotechnical Journal*, 55(1):45–56.

Tran, H. T., Wang, Y., Nguyen, G. D., Kodikara, J., Sanchez, M., and Bui, H. H. (2019). Modelling 3D desiccation cracking in clayey soils using a size-dependent SPH computational approach. *Computers and Geotechnics*, 116.

Vardoulakis, I. (1989). Shear-banding and liquefaction in granular materials on the basis of a Cosserat continuum

theory. *Ingenieur-Archiv*, 59(2):106–113.

Vardoulakis, I., Goldscheider, M., and Gudehus, G. (1978). Formation of shear bands in sand bodies as a bifurcation problem. *International Journal for Numerical and Analytical Methods in Geomechanics*, 2(2):99–128.

Vardoulakis, I. and Sulem, J. (1995). *Bifurcation Analysis in Geomechanics*. Blackie Academic and Professional.

Verma, R. K., Nguyen, G. D., Bui, H. H., and Karakus, M. (2021). Effect of specimen size on localization using digital image correlation. In Abdel Wahab, M., editor, *Proceedings of the 8th International Conference on Fracture, Fatigue and Wear*, pages 397–405, Singapore. Springer Singapore.

Wang, Y., Bui, H. H., Nguyen, G. D., and Ranjith, P. G. (2019). A new SPH-based continuum framework with an embedded fracture process zone for modelling rock fracture. *International Journal of Solids and Structures*, 159:40–57.

Wang, Y., Tran, H. T., Nguyen, G. D., Ranjith, P. G., and Bui, H. H. (2020). Simulation of mixed-mode fracture using SPH particles with an embedded fracture process zone. *International Journal for Numerical and Analytical Methods in Geomechanics*, 44(10):1417–1445.

Wells, G. N. and Sluys, L. J. (2001). A new method for modelling cohesive cracks using finite elements. *International Journal for Numerical Methods in Engineering*, 50(12):2667–2682.

Xu, G. and Pietruszczak, S. (1997). Numerical analysis of concrete fracture based on a homogenization technique. *Computers & Structures*, 63(3):497–509.

Ziegler, H. (1983). *An Introduction to Thermomechanics (2nd Ed.)*. North Holland, Amsterdam.

Manuscript received 4th September 2021, revised 2nd May 2022 and 16th June 2022, accepted 5th July 2022.